Design and Characterization of a 120-GHz Millimeter-Wave Antenna for Integrated Photonic Transmitters

Akihiko Hirata, Hiromu Ishii, and Tadao Nagatsuma, *Member, IEEE*

***Abstract*—We developed a planar slot antenna on an Si substrate for a photonic >100-GHz millimeter-wave (MMW) transmitter. We designed the antenna by using three-dimensional electromagnetic-field simulators and characterized its performance by using an optoelectronic network analyzer. The transmitter uses a very fast photodiode with high output power. Using these photonic techniques, we succeeded in building this compact photonic transmitter that emits MMWs with a power of >0.2 mW at a frequency of 120 GHz.**

***Index Terms*—Antenna, millimeter wave, photonic transmitter.**

I. Introduction

MILLIMETER-WAVE (MMW) radio has been attracting a great deal of attention as a way of meeting an increasing demand for broad-band wireless communication. For example, intensive research has been done to develop a wireless link using the 60-GHz band, which, by virtue of high atmospheric absorption, allows the formation of picocells with radii of the order of 100 m [1], [2]. However, the frequency region of above 100 GHz has not yet been exploited because generation and long-haul transmission of MMWs by an all-electronic system are rather difficult. Radio-on-fiber is expected to be the most promising system to enable overcoming these problems because it is much easier to generate high-frequency signals optically than electronically, and fiber-based systems use optical-fiber amplifiers and have a low transmission loss and a wide bandwidth [3], [4]. Since photonic transmitters are key components in these systems, many studies have reported on the development of such transmitters [5]–[7]. However, a photonic transmitter operating at a frequency of >100 GHz has not yet been developed because of the limitations in performance characterization method and design techniques. The bandwidth of commercially available full-band vector-network analyzers is only 110 GHz, and their extended versions operate within limited bands, such as 110–170 or 70–230 GHz [8]. A complex method is needed to characterize antenna performance at very high frequencies. As for the design, MMW antennas are commonly designed by using three-dimensional (3-D) electromagnetic-field simulators, the accuracy of which at a frequency of >100 GHz has not yet been clearly determined because of the above problems with characterization.

Manuscript received February 23, 2001.

The authors are with the NTT Telecommunication Energy Laboratories, Atsugi-shi, Kanagwa 243-0198, Japan (e-mail: ahirata@aecl.ntt.co.jp).

Publisher Item Identifier S 0018-9480(01)09376-0.

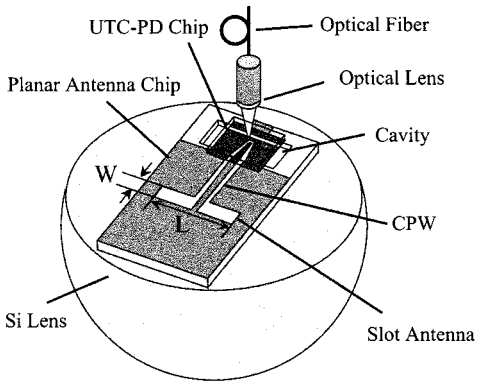

Fig. 1. Conceptual diagram of a proposed MMW photonic transmitter.

In this paper, we describe the design and characterize the performance of an >10-GHz MMW antenna for photonic transmitters. We designed the MMW antenna by using 3-D electromagnetic-field simulators and characterized its performance by using our >300-GHz-bandwidth optoelectronic network analyzer (ONA), which is based on an electrooptic sampling (EOS) technique [9]. We compared our measured results with the simulated ones to verify the accuracy of the simulators at a frequency of >100 GHz. We then fabricated a photonic transmitter by integrating a photodetector, a planar antenna, a hemispherical Si lens, and an optical fiber. For the MMW photodetector, we used a unitraveling-carrier photodiode (UTC–PD) [10]. This UTC–PD is a very fast photodiode (PD), capable of generating a high output power at frequencies within the MMW region [11]. The hemispherical Si lens collimates the MMWs from the antenna improving its gain and directivity. By using these techniques, we succeeded in detecting >0.2-mW output power emitted from the photonic transmitter.

II. Antenna Design

Fig. 1 shows the diagram of the designed photonic MMW transmitter. The transmitter consists of a planar antenna chip, a UTC–PD chip, a hemispherical Si lens, and an optical fiber with a collimating lens. We used a coplanar-waveguide-fed (CPW-fed) slot antenna for the planar antenna chip because it has an antenna pattern perpendicular to the substrate and is suitable for the connection of planar-active devices [12]. The slot antenna and CPW were formed on an Si substrate ($\varepsilon r = 11.7$), which was 0.4-mm thick. To decrease the dispersion and radiation loss due to the substrate, we used

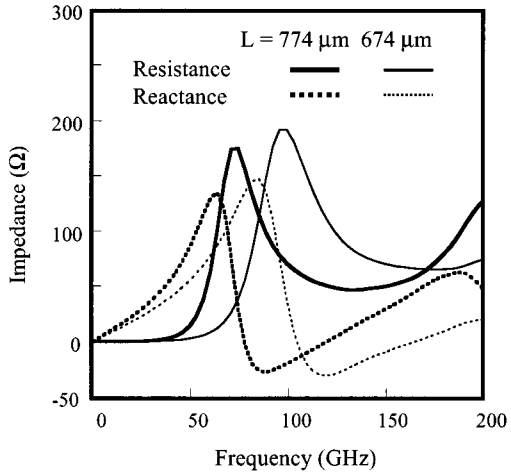

Fig. 2. Antenna-impedance simulation results as a function of slot length (L). Slot width (W) was kept at 95 μm. This simulation used the FDTD method.

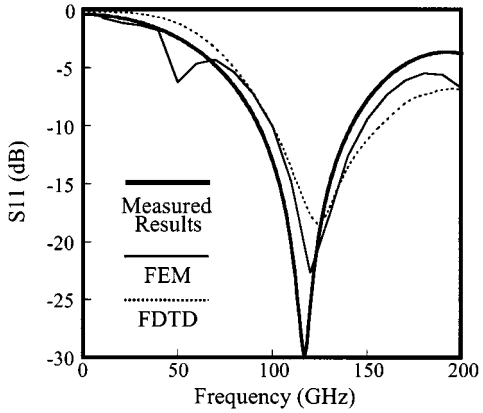

Fig. 3. Simulation and measurement results for input return loss $S11$.

high-resistivity Si and thick gold. The resistivity of the Si was 1 k$\Omega\cdot$cm, and the thickness of the gold was 10 μm. The signal linewidth of the CPW was 20 μm, the signal–ground space was 24 μm, and the impedance of the CPW was 50 Ω.

The fabrication process of this antenna was based on the Si-micromachining technology [13]. We formed a cavity on the Si antenna chip by anisotropic wet etching using a KOH solution. After the cavity formation, polyimide was spin coated to fill the cavity. We then removed the polyimide outside the cavity by chemical mechanical planarization (CMP) to planarize the surface of the substrate. Gold patterns were then formed by electroplating. Finally, the polyimide in the cavity was removed by dry etching.

The UTC–PD chip was flip-chip bonded over the cavity to avoid the effects of the Si substrate on the impedance of the transmission line in the UTC–PD chip. The depth of the cavity was 20 μm, and the height of the CPW pads in the antenna chip was 10 μm. Thus, the distance between the antenna–chip surface and the UTC–PD–chip surface was 30 μm. Optical signals were injected into the UTC–PD. The resulting electrical signals traveled along the CPW to the slot antenna. This produced MMW signals, which were collimated by the Si lens and radiated into free space.

For the antenna design, we used two different 3-D electromagnetic simulators. One was based on the finite-element method (FEM), and the other was based on the finite-difference time-domain (FDTD) method. First, we simulated the impedance of the slot antenna to determine the antenna geometry by using the FDTD method. The impedance of the CPW was assumed to be 50 Ω, and the target frequency was 120 GHz. Thus, the resistance should be 50 Ω, and the reactance should be 0 Ω at the frequency of 120 GHz. The simulation results for the antenna impedance are presented in Fig. 2 for different slot lengths (L) and slot widths (W). This simulation was done by using the FDTD method. When L was 774 μm and W was 95 μm, the reactance became zero, and the resistance was 50 Ω at 120 GHz. When L was 674 μm and W was 95 μm, the antenna resonated at 166 GHz, and the impedance became 66 Ω. In contrast, when W was reduced to 75 μm and L was kept at 774 μm, the impedance decreased to 38 Ω at a resonant frequency of 125 GHz. Thus, the resonant frequency mainly depended on the slot length, while the impedance depended on the slot width. Based on these simulation results, we determined the dimensions of the 50-Ω slot antenna where L was 774 μm, and W was 95 μm.

The accuracy of the simulation was verified by comparing our measured results with the simulated ones. We measured the input return loss $S11$ of the antenna by using an ONA. We also did a number of simulations using the FEM. The measurement and simulation results are shown in Fig. 3. The FEM and FDTD simulators predicted the resonant frequency to be 120 and 124 GHz, respectively. The measured resonant frequency was 117 GHz, with a return loss of -29.9 dB. This is fairly close to the simulation results, which confirms the accuracy of the simulations at frequencies of above 100 GHz. The measured bandwidth for a 10-dB return loss was 49 GHz (41%), while the bandwidth obtained by the simulations was 46 GHz (39%) for the FEM simulator and 53 GHz (43%) for the FDTD simulator. Thus, we were able to design a broad-band antenna that can be used for broad-band wireless communication.

Next, we investigated the effects of the Si lens. The Si lens synthesizes an infinite Si substrate, thus eliminating substrate-mode excitation and the associated power loss in these modes [14]. The slot antenna placed on the infinite Si substrate radiates preferentially into the substrate with a ratio of $\varepsilon r^{3/2}$ over the power radiated into the air side [7]. The hemispherical lens collimates the MMWs radiated from the slot antenna [15]. The extension length of the hemispherical lens was determined in the FEM simulation to ensure the maximum directivity of the transmitter. We determined that the extension length of the hemispherical Si lens was 1.9 mm, and the diameter of the lens was 10 mm.

Fig. 4 shows radiation patterns of the antenna calculated by the FEM. In this simulation, the Si lens was modeled by a full space. Without the Si lens, the power radiated into both the air and substrate sides. When the Si lens was used, most of the power radiated into the substrate side, and the beam was collimated toward the axis perpendicular to the substrate.

Table I shows the simulated antenna parameters with and without the Si lens. The Si lens significantly improved both the

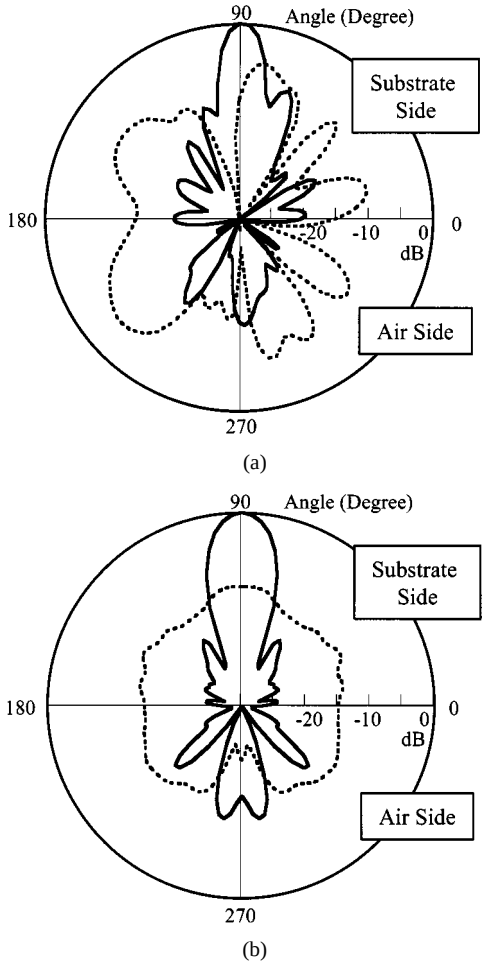

Fig. 4. Radiation patterns of slot antenna with and without the Si lens calculated by the FEM: (a) in the E-plane and (b) in the H-plane. The solid lines show the radiation pattern of the antenna with the Si lens, and the dotted lines show that without the Si lens.

TABLE I
GAIN AND DIRECTIVITY OF THE MMW ANTENNA WITH AND WITHOUT SI LENS

	With Lens	W/O Lens
Gain	13.5 dB	4.3 dB
Directivity (dB)	16.9 dB	4.9 dB

gain and directivity of the antenna. With the lens, gain and directivity of the antenna were 13.5 and 16.9 dB, respectively. Thus, by using an Si lens, we can detect much higher power along the axis perpendicular to the substrate, which is useful for directive wireless communication. There was approximately 3-dB difference between the directivity and gain of the antenna. The difference comes from the transmission loss at the CPW, the dielectric loss in the Si lens, and the reflection loss at the Si lens–air interface. We measured the transmission loss of the CPW, which was about 0.6 dB. Therefore, we suppose that the major loss was caused by the dielectric loss in the Si lens and the reflection loss at the Si lens–air interface.

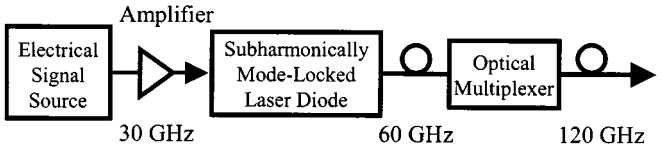

Fig. 5. Optical 120-GHz MMW source.

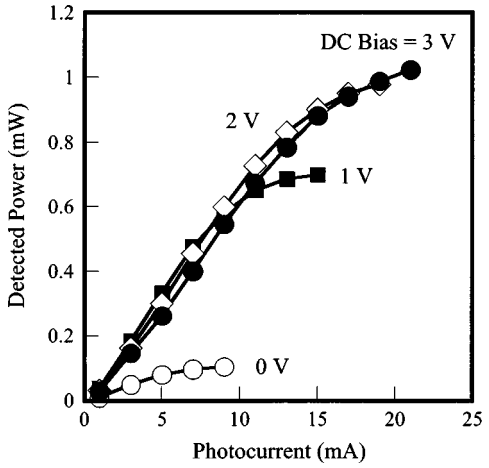

Fig. 6. Dependence of detected 120-GHz output power of the UTC–PD on photocurrent as a function of dc-bias voltage.

III. EXPERIMENTAL RESULTS

A. UTC–PD Output Power

We measured the output power of the UTC–PD on a wafer at a frequency of 120 GHz. Optical signals with a frequency of 120 GHz (1.55 μm) were generated by an optical MMW source and were delivered with optical fiber. They were focused onto the UTC–PD made on an InP wafer from the backside of the wafer. The output power of the UTC–PD was transmitted to the waveguide detector by a MMW probe. The waveguide detector used a calibrated Schottky barrier diode.

A schematic diagram of the 120-GHz MMW optical source used in this experiment is shown in Fig. 5. The optical signals were generated by a mode-locked laser diode (ML–LD) integrated with an electro-absorption modulator [16]. The ML–LD was driven at 30 GHz, and second harmonic 60-GHz repetitive-frequency pulse trains were generated. The optical signals were frequency doubled to 120 GHz using an optical multiplexer and then boosted with an optical fiber amplifier.

Fig. 6 shows the dependence of the detected UTC–PD output power on the photocurrent $(I_{\rm ph})$. The diameter of the UTC–PD was 8 μm and the 3-dB bandwidth of this UTC–PD measured by the time-domain pulse response was 95–100 GHz. The detected power first increased with an increase in $I_{\rm ph}$, and then saturated. The saturation began at lower $I_{\rm ph}$, as the dc-bias voltage $(V_{\rm bias})$ became lower. This mainly comes from the nonlinear saturation of the UTC–PD at frequencies beyond its 3-dB bandwidth. The maximum output power of this UTC–PD exceeds 1.0 mW ($I_{\rm ph} = 21$ mA, $V_{\rm bias} = 3$ V).

B. Photonic-Transmitter Characteristics

Fig. 7(a) and (b) shows photographs of the photonic transmitter before integration of an optical fiber. In Fig. 7(a), the

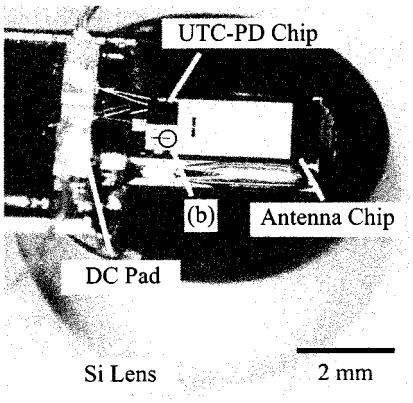

(a)

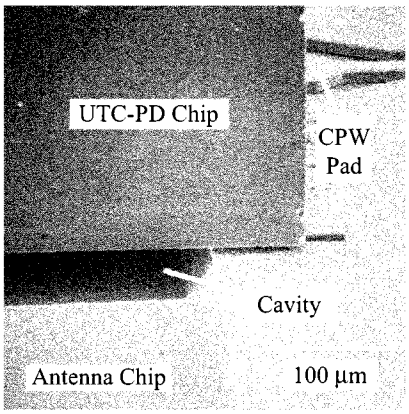

(b)

Fig. 7. (a) Fabricated photonic transmitter before integration of optical fiber and package. (b) SEM micrograph of cavity formed on the planar antenna chip. This micrograph shows the area inside the black circle in Fig. 7(a).

UTC–PD chip was flip-chip bonded on the CPW pad of the antenna chip. The size of the antenna chip and that of the UTC–PD chip was 2×4 mm and 0.6×0.8 mm, respectively. The planar slot antenna was centered on the Si lens. DC pads and leads were installed for bias-voltage application. Fig. 7(b) shows a secondary electron microscopy (SEM) micrograph of the cavity formed on the Si antenna chip. A 20-μm-deep cavity was formed on the Si substrate. The UTC–PD chip was flip-chip bonded over the cavity, and there was an air gap between the UTC–PD and antenna chips. Fig. 8 shows the transmitter after the integration of the optical fiber and after it was packaged in a metal package. The components, except for the Si lens and the optical fiber, are in the metal package. The diameter and height of the module are 20 mm.

First, the radiation pattern of the photonic transmitter was measured. The measurement and FEM-simulation results are shown in Fig. 9. The radiated power was collimated very well along the axis almost perpendicular to the substrate. The 3-dB beamwidths of the transmitter for the E- and H-planes were 13° and 8°, respectively, and the sidelobe levels remains below -10 dB. These results indicate that the Si lens worked very well. These measured results also corresponded to the simulated ones at a frequency of over 100 GHz.

Next, we measured the output power of the photonic transmitter. The setup for measuring the output power of the photonic

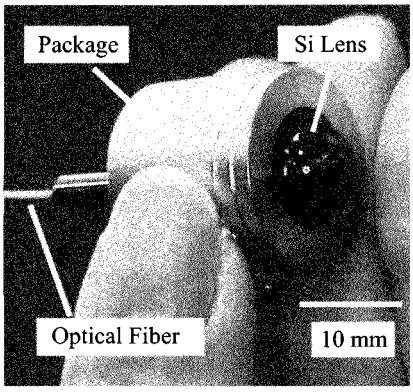

Fig. 8. Fabricated photonic transmitter after integration of optical fiber and package.

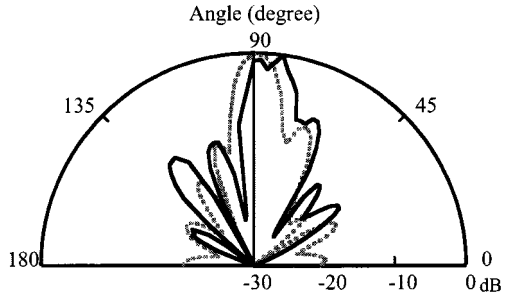

(a)

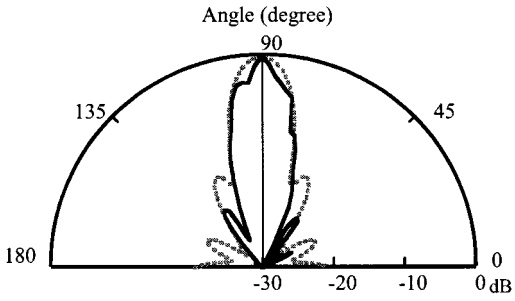

(b)

Fig. 9. Radiation patterns of the photonic transmitter for the: (a) E- and (b) H-planes. The solid lines show the measurement results and the dotted lines show simulation results.

transmitter is shown in Fig. 10. Optical MMW signals were delivered to the photonic transmitter with an optical fiber cable. The radiated power from the transmitter was collimated and focused on the horn antenna by two Teflon lenses. The received MMW power was measured by the same waveguide detector used for the UTC–PD output-power measurement.

Fig. 11 shows the dependence of the detected power on $I_{\rm ph}$. The detected power increased and then leveled off as $I_{\rm ph}$ increased. Saturation of the output power began at lower $I_{\rm ph}$ as $V_{\rm bias}$ became lower. This is similar to the characteristics of the UTC–PD output power. Small differences in the two data sets seem to be due to the fact that the relationship between the output power and $I_{\rm ph}$ slightly depends on the focusing conditions of the laser beam on the PD. Optimum focus conditions could not be achieved in the assembly. The maximum detected power of the transmitter was about 0.25 mW when $I_{\rm ph}$ was 21 mA and $V_{\rm bias}$ was 3 V. Not all of the radiated power could

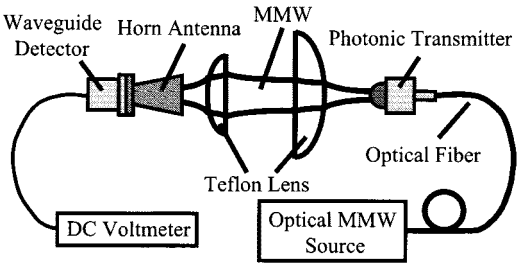

Fig. 10. Experimental setup for the output-power measurement of the photonic transmitter.

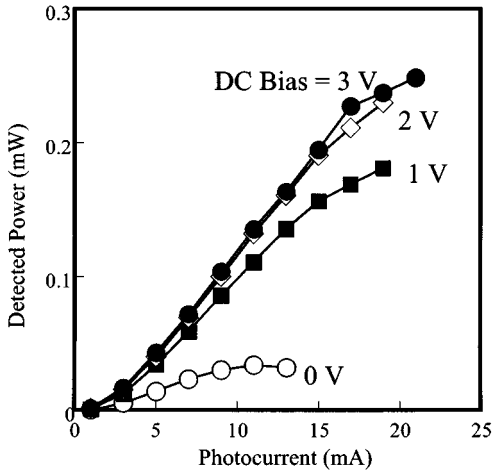

Fig. 11. Dependence of detected MMW output power of the photonic transmitter on photocurrent as a function of dc-bias voltage.

be detected by the setup shown in Fig. 10. For example, the loss at the two Teflon lenses is estimated to be about 3.6 dB, which indicates that the actual radiated power was at least over 0.57 mW. Moreover, this transmitter emitted MMWs with a power of >30 μW without applying dc-bias voltage. To our knowledge, this is the first time that the MMW power emitted into free space from a PD-integrated antenna was detected at a frequency of over 100 GHz.

IV. Conclusion

We developed >100-GHz planar slot antenna for photonic transmitters. We designed the antenna by using 3-D electromagnetic-field simulators and characterized its performance by using an ONA. The measured results corresponded to the simulated ones, confirming the accuracy of our simulation at a frequency of over 100 GHz. The MMW antenna was integrated with a UTC–PD, a hemispherical Si lens, and an optical fiber to form a photonic MMW transmitter. We found that the UTC–PD can produce so much power that electrical amplifiers become unnecessary, which makes the transmitter module very compact. The maximum detected output power of the transmitter was 0.25 mW. To our knowledge, this is the first time that the output power of a photonic antenna driven by a PD has been detected at a frequency of over 100 GHz. Our results demonstrate that this transmitter can be effectively used for broad-band wireless communications.

Acknowledgment

The authors are grateful to Dr. T. Ishibashi, NTT Photonics Laboratories, Atsugi-shi, Kanagawa, Japan, and Dr. T. Furuta, NTT Photonics Laboratories, Atsugi-shi, Kanagawa, Japan, for supplying the UTC–PDs, and to Dr. N. Sahri, NTT Telecommunications Energy Laboratories, Atsugi-shi, Kanagawa, Japan, for designing and characterization of antennas. The authors would also like to thank Dr. K. Machida, NTT Telecommunications Energy Laboratories, Atsugi-shi, Kanagawa, Japan, Dr. H. Kyuragi, NTT Telecommunications Energy Laboratories, Atsugi-shi, Kanagawa, Japan, and Dr. J. Yamada, NTT Telecommunications Energy Laboratories, Atsugi-shi, Kanagawa, Japan, for their useful discussions and encouragement.

References

[1] K. Ohata, K. Maruhashi, J. Matsuda, M. Ito, W. Domon, and S. Yamazaki, "A 500 Mbps 60 GHz-band transceiver for IEEE 1394 wireless home network," in *European Microwave Conf. Tech. Dig.*, 2000, pp. 290–293.

[2] K. Hamaguchi, Y. Shoji, H. Ogawa, H. Sato, K. Totuda, Y. Hirachi, T. Iwasaki, A. Akeyama, K. Ueki, and T. Kizawa, "A wireless video home-link using 60 GHz band: Concept and performance of developed system," in *European Microwave Conf. Tech. Dig.*, 2000, pp. 294–297.

[3] K. Ogusu, K. Inagaki, and Y. Mizuguchi, "400 Mbit/s BPSK data transmission at 60 GHz-band mm-wave using a two-mode injection-locked Fabry–Perot slave laser," in *Microwave Photon. Technol. Dig.*, 2000, pp. 31–34.

[4] S. Iezekiel and N. Bourrhill, "Optical control of millimeter-wave p-HEMT's with application to fiber radio," in *Microwave Photon. Technol. Dig.*, 2000, pp. 55–58.

[5] D. Ferling, W. Heinrich, W. Kuebart, G. Luz, and F. Buchali, "Hybrid integrated fiber-amplifier-antenna module for radio applications at 60 GHz," in *IEEE MTT-S. Int. Microwave Symp. Dig.*, 1999, pp. 457–460.

[6] G. A. Chakam and W. Freude, "Coplanar phased array antenna with optical feeder and photonic bandgap structure," in *Microwave Photon. Technol. Dig.*, 1999, pp. 1–4.

[7] K. Takahata, Y. Muramoto, S. Fukushima, T. Furuta, and H. Ito, "Monolithically integrated millimeter-wave photonic emitter for 60-GHz fiber-radio application," in *Microwave Photon. Technol. Dig.*, 2000, pp. 229–232.

[8] O. Wohlgemuth, M. J. Rodwell, R. Reuter, J. Braunstein, and M. Schlechtweg, "Active probes for network analysis within 70–230 GHz," *IEEE Trans. Microwave Theory Tech.*, vol. 47, pp. 2591–2598, Dec. 1999.

[9] N. Sahri and T. Nagatsuma, "Packaged photonic probes for an on-wafer broad-band millimeter-wave network analyzer," *IEEE Photon. Technol. Lett.*, vol. 12, pp. 1225–1227, Sept. 2000.

[10] T. Ishibashi, N. Shimizu, S. Kodama, H. Ito, T. Nagatsuma, and T. Furuta, "Uni-traveling-carrier photodiodes," in *Ultrafast Electron. Optoelectron. Tech. Dig.*, 1997, pp. 166–169.

[11] T. Nagatsuma, N. Sahri, M. Yaita, T. Ishibashi, N. Shimizu, and K. Sato, "All optoelectronic generation and detection of millimeter-wave signals," in *Microwave Photon. Technol. Dig.*, 1998, pp. 5–8.

[12] B. K. Kormanyos, W. Harokopus, L. P. B. Katehi, G. M. Rebeiz, and M. Rebeiz, "CPW-fed active slot antennas," *IEEE Trans. Microwave Theory Tech.*, vol. 42, pp. 541–545, Apr. 1994.

[13] H. Ishii, N. Sahri, T. Nagatsuma, K. Machida, K. Saito, S. Yagi, M. Yano, K. Kudo, and H. Kyuragi, "A new fabrication process for low-loss millimeter-wave transmission lines on silicon," in *Extended Abstract Int. Solid State Devices Mater. Conf.*, 1999, pp. 126–127.

[14] D. B. Rutledge, D. P. Neikrik, and D. P. Kasilingam, *Integrated Circuit Antennas in Infrared and Millimeter-Waves*, K. J. Button, Ed. New York: Academic, 1983, vol. 10, pp. 1–90.

[15] D. F. Filipovic, S. S. Gearhart, and G. M. Rebeiz, "Double-slot antennas on extended hemispherical and elliptical silicon dielectric lens," *IEEE Trans. Microwave Theory Tech.*, vol. 41, pp. 1738–1749, Oct. 1993.

[16] K. Sato, I. Kotaka, Y. Kondo, and M. Yamamoto, "Active mode-locking at 50-GHz repetition frequency by half-frequency modulation of monolithic semiconductor lasers integrated with electro-absorption modulators," *Appl. Phys. Lett.*, vol. 69, pp. 2626–2628, 1996.

Akihiko Hirata was born in Kyoto, Japan, on August 24, 1968. He received the B.S. and M.S. degrees in chemistry from Tokyo University, Tokyo, Japan, in 1992 and 1994, respectively.

In 1994, he joined the large-scale integration (LSI) Laboratories (now the NTT Telecommunications Energy Laboratories), Nippon Telegraph and Telephone Corporation (NTT), Kanagawa, Japan. His current research involves MMW antenna and photonic technology.

Mr. Hirata is a member of the Japan Society of Applied Physics.

Hiromu Ishii was born in Nikko, Japan, in 1956. He received the B.S., M.S., and Ph.D. degrees in physical chemistry from the University of Tokyo, Tokyo, Japan, in 1982, 1984, and 1996, respectively.

In 1984, he joined the NTT Atsugi Electrical Communications Laboratories (now the NTT Telecommunications Energy Laboratories), Kanagawa, Japan. He is an Associate Editor for the *Japanese Journal of Applied Physics*. He has been engaged in research and development of nanoscale film growth technologies focusing on atomic layer epitaxy of group-IV semiconductors by controlling surface chemical reactions, development of ultra-large-scale integration (ULSI)-contact metallization techniques using metal–chemical–vapor deposition and multilevel interconnection processes for CMOS/separation by implanted oxygen (SIMOX) LSIs. He is currently involved with the development of new integration technologies for high-speed Si systems based on microelectromechanical systems (MEMS).

Dr. Ishii is a member of the Japan Society of Applied Physics, the Physical Society of Japan, and the Chemical Society of Japan.

Tadao Nagatsuma (M'93) received the B.S., M.S., and Ph.D. degrees in electronic engineering from Kyushu University, Fukuoka, Japan, in 1981, 1983, and 1986, respectively.

In 1986, he joined the Atsugi Electrical Communications Laboratories (now the NTT Telecommunications Energy Laboratories), Nippon Telegraph and Telephone Corporation (NTT), Kanagawa, Japan, where he is currently a Distinguished Technical Member, Senior Research Scientist, and Supervisor. His current research involves ultra-high-speed electronics and MMW photonics, and their application to sensors and communications.

Dr. Nagatsuma is a member of the Optical Society of America, the Japan Society of Applied Physics, and the Institute of Electronics, Information and Communication Engineers (IEICE), Japan. He was the recipient of the 1989 Young Engineers Award presented by the IEICE, the 1992 IEEE Andrew R. Chi Best Paper Award, the 1997 Okochi Memorial Award, the 1998 Japan Microwave Prize, and the 2000 Minister's Award of the Science and Technology Agency.